A Stochastic Model of the Temporal and Azimuthal Dispersion Seen at the Base Station in Outdoor Propagation Environments

Klaus Ingemann Pedersen, Preben E. Mogensen, and Bernard H. Fleury

***Abstract*—A simple statistical model of azimuthal and temporal dispersion in mobile radio channels is proposed. The model includes the probability density function (pdf) of the delay and azimuth of the impinging waves as well as their expected power conditioned on the delay and azimuth. The statistical properties are extracted from macrocellular measurements conducted in a variety of urban environments. It is found that in typical urban environments the power azimuth spectrum (PAS) is accurately described by a Laplacian function, while a Gaussian pdf matches the azimuth pdf. Moreover, the power delay spectrum (PDS) and the delay pdf are accurately modeled by an exponential decaying function. In bad urban environments, channel dispersion is better characterized by a multicluster model, where the PAS and PDS are modeled as a sum of Laplacian functions and exponential decaying functions, respectively.**

***Index Terms*—Antenna arrays, azimuth dispersion, directional channel model, propagation model.**

I. Introduction

ADVANCED diversity and spatial filtering schemes are some of the potential techniques which can significantly increase the capacity of terrestrial cellular systems. Indeed, implementation of antenna arrays at the base station (BS) is expected to yield a significant capacity gain [1], [2]. The optimum antenna array topology and combining algorithm are strongly related to the behavior of the radio channel and especially to its azimuth dispersion. As an example, if conventional beamforming techniques are applied, the beamwidth should be adjusted in such a way that it captures most of the impinging power, i.e., the beamwidth should be adapted to the degree of azimuth dispersion in the channel. If the goal is to steer a null in the direction of an interfering user, the required null width is also determined by the extent of azimuth dispersion. Azimuth dispersion furthermore determines the correlation between the output signals at two specific spatially separated antennas and consequently the ability to mitigate fast fading by means of antenna diversity techniques. The spatial properties of the channel therefore have an enormous impact on the performance of antenna array systems and, hence, need to be well characterized in order to make it possible to design efficient radio communication systems in the future.

At present, generally accepted wide-band radio channel models [3]–[6] characterize only temporal dispersion and are therefore considered to be too simple to test advanced antenna array systems, since the azimuth dispersion is missing. Previous studies of azimuth dispersion at the BS have either been based on measurements or simple geometric models [7]. Estimates of the azimuth spread obtained in different environments are reported in [8]–[10]. Simple analytical two-dimensional (2-D) models have been proposed in [11] and [12], and a more advanced three-dimensional (3-D) single scattering model which takes the antenna height into account is reported in [13]. However, most of these models still need to be validated by measurements.

In this study, a simple stochastic radio channel model is proposed which includes both temporal and azimuthal dispersion. Functions which characterize the random behavior of the model parameters are extracted from experimental data collected during extensive measurement campaigns in Aarhus, Denmark, and Stockholm, Sweden. We have classified these environments as typical and bad urban macrocellular. The model parameters are extracted from measurements performed at elevated BS antennas only. Notice that there is a fundamental difference between azimuth dispersion observed at an elevated BS and a mobile station (MS) even though the propagation channel is assumed to be reciprocal. It is often assumed that the incoming azimuthal field distribution at the MS can be modeled by a uniform probability density function (pdf) as discussed in [14]–[16], among others. This model is commonly called Clarke's model. At an elevated BS, the incoming field is expected to be more concentrated in azimuth since the BS antenna is located well above surrounding scatterers [8]. The consequences of these differences are discussed more thoroughly within the paper as the results are presented.

The paper is organized as follows. In Section II, the radio channel model is outlined. The measurement system, the signal processing method used to estimate the channel parameters, and the investigated environments are described in Section III. Sections IV–VII present the results from the extensive measurement campaigns, and finally some concluding remarks are given in Section VIII.

Manuscript received April 25, 1998; revised June 24, 1999. This work was supported by the Danish Technical Research Council, the European Union (ACTS, TSUNAMI II), Nokia Telecommunications, and Ericsson Radio Systems AB.

The authors are with the Center for PersonKommunikation, Aalborg University, DK-9220 Aalborg, Denmark (e-mail: kip@cpk.auc.dk; pm@cpk.auc.dk; bfl@cpk.auc.dk).

Publisher Item Identifier S 0018-9545(00)02554-8.

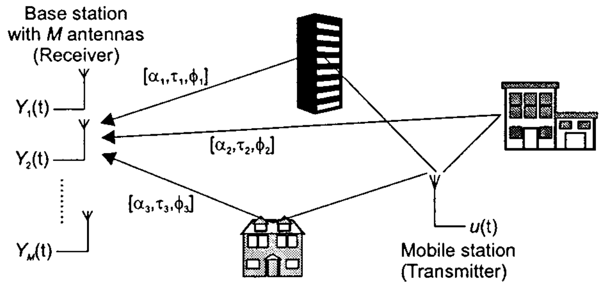

Fig. 1. Illustration of the used signal model with $L = 3$ waves.

II. Stochastic Model

Due to multipath propagation in the radio channel, several replicas of the transmitted signal are received from different directions and/or with different time delays as illustrated in Fig. 1. Thus, the received baseband signal vector sensed by an uniform linear antenna array can be expressed as

$$\mathbf{Y}(t) = \sum_{\ell=1}^{L} \alpha_\ell \mathbf{c}(\phi_\ell) u(t - \tau_\ell) + \mathbf{N}(t). \tag{1}$$

The components in $\mathbf{Y}(t) = [Y_1(t), Y_2(t), \cdots, Y_M(t)]^T$ are the signals at the output of the M antenna elements and $u(t)$ is the transmitted sounding signal. The mathematical notation $[\cdot]^T$ denotes transposition. The parameters α_ℓ, τ_ℓ, and ϕ_ℓ are the complex amplitude, delay, and incidence azimuth of the ℓth impinging wave, respectively. The number of impinging waves is L. The array steering vector is expressed as $\mathbf{c}(\phi) = [c_1(\phi), c_2(\phi), \cdots, c_M(\phi)]^T$, with $c_m(\phi) = f_m(\phi)\exp[-j(m-1)2\pi d/\lambda \sin\phi]$, where $f_m(\phi)$ is the complex field pattern of the mth array element, d is the element spacing, and λ is the wavelength. The components of the noise vector $\mathbf{N}(t) = [N_1(t), N_2(t), \cdots, N_M(t)]^T$ are assumed to be independent complex white Gaussian noise processes with identical power density. The sum in (1) can be rewritten as an integral according to

$$\mathbf{Y}(t) = \iint \mathbf{c}(\phi) h(\phi, \tau) u(t - \tau)\, d\tau\, d\phi + \mathbf{N}(t) \tag{2}$$

with

$$h(\phi, \tau) = \sum_{\ell=1}^{L} \alpha_\ell \delta(\phi - \phi_\ell, \tau - \tau_\ell). \tag{3}$$

Extending Bello's terminology [9], we call $h(\phi, \tau)$ the azimuth-delay spread function of the channel. It should be emphasized that $h(\phi, \tau)$ is time variant since it changes as the MS moves. However, to simplify the notation we have omitted this dependency. All parameters in (3) are random variables. Randomness occurs since the constellation of the impinging waves is likely to change as the MS moves. Hence, $h(\phi, \tau)$ is a random process which is entirely described by the joint pdf of its random parameters. We furthermore assume that the random vectors $[\alpha_1, \tau_1, \phi_1], [\alpha_2, \tau_2, \phi_2], \cdots, [\alpha_L, \tau_L, \phi_L]$ are independent and identically distributed.

Based on the proposed model, let us define the instantaneous power azimuth-delay spectrum to be

$$P_I(\phi, \tau) = \sum_{\ell=1}^{L} |\alpha_\ell|^2 \delta(\phi - \phi_\ell, \tau - \tau_\ell) \tag{4}$$

where $|\cdot|$ denotes the absolute value of the argument. Notice that the terminology *spectrum* is adopted according to Proakis [17]. From (4) the power azimuth-delay spectrum is defined as

$$P(\phi, \tau) = E\{P_I(\phi, \tau)\} \tag{5}$$

where $E\{\cdot\}$ denotes expectation. The power azimuth spectrum (PAS) and the power delay spectrum (PDS) are derived from $P(\phi, \tau)$ according to

$$P_A(\phi) = \int P(\phi, \tau)\, d\tau \tag{6}$$

$$P_D(\tau) = \int P(\phi, \tau)\, d\phi. \tag{7}$$

The subscripts A and D refer to azimuth and delay domain, respectively. Let us furthermore define the azimuth spread (AS) σ_A as the root second central moment of $P_A(\phi)$ [8] and the delay spread (DS) σ_D as the root second central moment of $P_D(\tau)$ [17]. The joint pdf of the azimuths and delays is denoted by $f(\phi, \tau)$. Their marginal pdf's are

$$f_A(\phi) = \int f(\phi, \tau)\, d\tau \tag{8}$$

$$f_D(\tau) = \int f(\phi, \tau)\, d\phi \tag{9}$$

and their variances are denoted by $\tilde{\sigma}_A^2$ and $\tilde{\sigma}_D^2$, respectively. Based on these definitions, the conditional power azimuth-delay spectrum can be expressed as

$$P(\phi, \tau \,|\, \mathbf{a}) = \sum_{\ell=1}^{L} E\{|\alpha_\ell|^2\} \delta(\phi - \phi_\ell, \tau - \tau_\ell) \tag{10}$$

where $\mathbf{a} = [L, \phi_1, \tau_1, \phi_2, \tau_2, \cdots, \phi_L, \tau_L]$. From (10), the unconditional power spectrum is easily derived as

$$P(\phi, \tau \,|\, L) = \sum_{\ell=1}^{L} E\{|\alpha_\ell|^2 \,|\, \phi_\ell = \phi, \tau_\ell = \tau\} f(\phi, \tau) \tag{11}$$

$$P(\phi, \tau) = E\{L\} E\{|\alpha|^2 \,|\, \phi, \tau\} f(\phi, \tau) \tag{12}$$

$$\propto E\{|\alpha|^2 \,|\, \phi, \tau\} f(\phi, \tau) \tag{13}$$

where

$$E\{|\alpha|^2 \,|\, \phi, \tau\} = E\{|\alpha_\ell|^2 \,|\, \phi_\ell = \phi, \tau_\ell = \tau\}, \quad \text{for } \ell \in [1, 2, \cdots, L] \tag{14}$$

is the expected power of the waves conditioned on their azimuth and delay. The notation $a \propto b$ means that the two terms a and

b are proportional. From (13), the power azimuth-delay spectrum is proportional to the conditional expected power of the waves multiplied by the azimuth-delay pdf. Similarly, the PAS and PDS can be expressed as

$$P_A(\phi) \propto E\{|\alpha|^2 \,|\, \phi\} f_A(\phi) \tag{15}$$

$$P_D(\tau) \propto E\{|\alpha|^2 \,|\, \tau\} f_D(\tau) \tag{16}$$

where $E\{|\alpha|^2 \,|\, \phi\}$ and $E\{|\alpha|^2 \,|\, \tau\}$ are the expected powers of the waves conditioned on their azimuth and delay, respectively.

In the following $P(\tau,\phi)$, $P_A(\phi)$, $P_D(\tau)$, $f_A(\phi)$, $f_D(\tau)$, $E\{|\alpha|^2 \,|\, \phi\}$, $E\{|\alpha|^2 \,|\, \tau\}$, and the cumulative distribution function (cdf) of σ_A and σ_D are determined experimentally. In the experimental analysis, we need to compute an estimate of the expectation in (5). Estimates of $P(\phi,\tau)$ in (5) are obtained by averaging $P_I(\phi,\tau)$ over a distance of 100λ corresponding to 16 m at a carrier frequency of 1.8 GHz. Notice that in the current study, we only investigate the dispersive behavior of the radio channel seen from the BS antenna. Other important propagation mechanisms such as fast fading, slow fading, path loss, etc., are not considered in this paper.

III. Measurement Campaigns

A. Stand-Alone Testbed

The measurement campaign was conducted by using the wide-band stand-alone testbed developed within the European Union funded research project ACTS, TSUNAMI II (Technology in Smart antennas for UNiversal Advanced Mobile Infrastructure, Part II) [2]. The setup consists of a BS equipped with an eight-element uniform linear antenna array and a MS with an omnidirectional car-mounted antenna. The BS antenna array (see Fig. 2) is constructed of vertically polarized dipole elements mounted in front of a ground plane. There is a total of 10×4 elements (horizontal $\times$ vertical) where the four vertical elements in each column are passively combined in order to achieve a larger antenna gain. The horizontal element spacing is half of a wavelength. The two outer element columns are terminated to a passive load in order to obtain an approximately uniform coupling across the array elements, i.e., to reduce the edge effects. The resulting array structure has a front-to-back ratio in excess of 28 dB so the well-known $\pm 180°$ ambiguity problem in the azimuth estimation can be neglected in practice [2]. The MS is equipped with a differential global positioning system (GPS) and an accurate position encoder so its location is known at any time during the measurement campaign. The system is designed for uplink transmission, i.e., from the MS to the BS. Simultaneous channel sounding is performed on all eight antenna branches which makes it possible to estimate the azimuth of the impinging waves at the BS, since all eight receiver branches are fully calibrated. The sounding signal $u(t)$ is a maximum length linear shift register sequence of length $K = 127$ chips. The testbed operates at a carrier frequency of 1.8 GHz and the chip rate equals $1/T_c = 4.096$ Mcps. Thus, the bandwidth of the sounding signal is comparable to the bandwidth used by the recently selected wide-band CDMA third-generation cellular system [18]. The received signals at the output of the antenna array are simultaneously sampled every $T_s = T_c/2 = 122$ ns and recorded for further off-line processing.

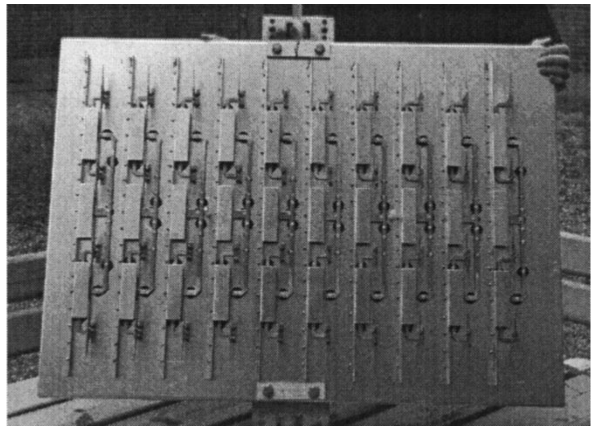

Fig. 2. Picture of the 10×4 element antenna array.

B. Investigated Environments

One of the urban measurement campaigns was conducted in Aarhus, Denmark, which is an area characterized by buildings ranging from four to six floors and an irregular street grid. No buildings are significantly higher than the average building height. Measurements were carried out every half wavelength ($\lambda/2 = 80$ mm) along six different routes having an average length of 2 km. All measurements were repeated twice with the BS antenna mounted at two different heights: 20 and 32 m. The lowest height corresponds to the average rooftop level of the surrounding buildings. In most cases, there was no line-of-sight (LOS) between the MS and BS.

Urban measurements were also collected in Stockholm, Sweden. In the investigated areas buildings are between four–six floors tall and placed on a slightly rolling terrain. The BS antenna was mounted 21 m above ground level, which corresponds to the average rooftop level of the surrounding buildings. Measurements were performed with the BS antenna pointing in two different directions as shown in Fig. 3. Here, the direction of the antenna array refers to the direction perpendicular to the array elements, i.e., the broadside direction. Direction #1 covers an area which is a mixture of a densely built-up zone and an open flat area represented by the river.

We classify Aarhus and Stockholm (direction #2) as typical urban environments, since time dispersion in these areas is similar to that of the COST207 typical urban model [6]. Time dispersion in Stockholm (direction #1) is similar to that of the COST207 bad urban environment, so we will refer to this area as bad urban. In the sequel, all results obtained from the Stockholm measurements are implicitly referring to direction #2 (typical urban), unless explicitly mentioned.

C. Estimation of the Channel Parameters

The parameters of each impinging wave in (3) are estimated from the received baseband signal vector $\mathbf{Y}(t)$ by using the space alternating generalized expectation maximization (SAGE) algorithm [19]. Basically, this scheme provides a

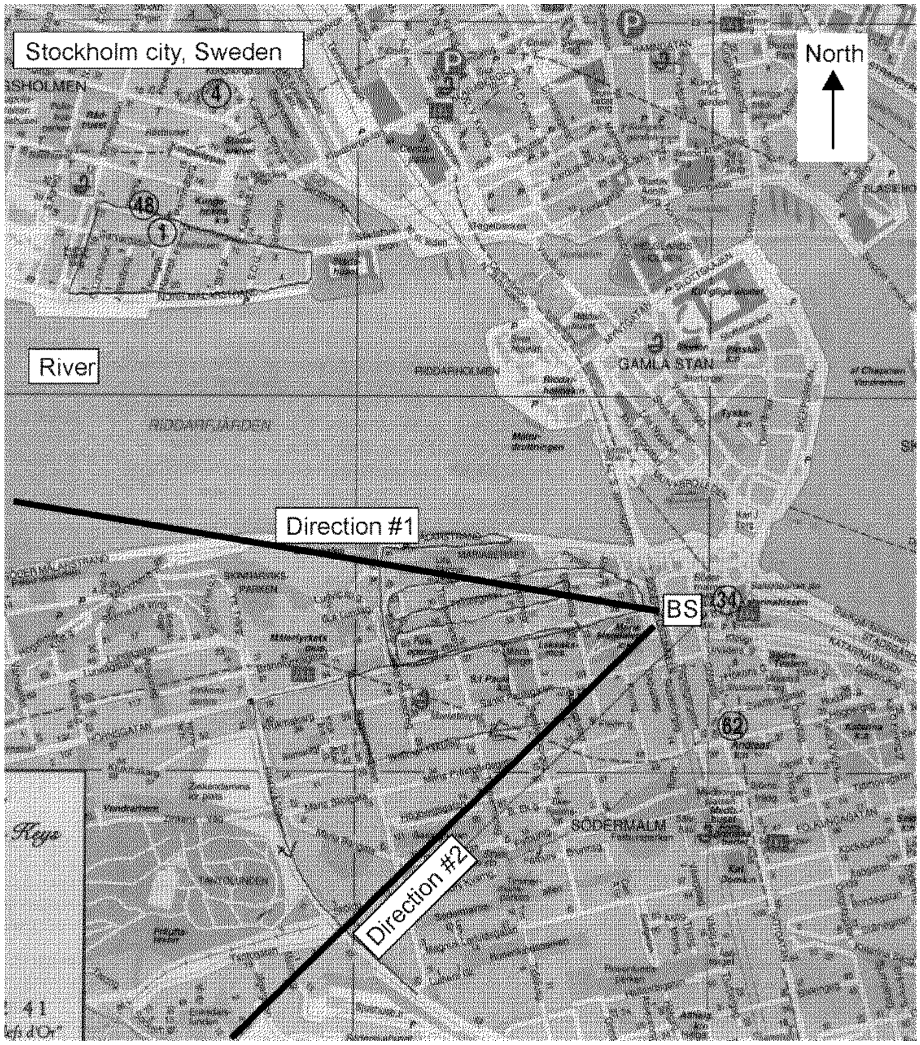

Fig. 3. Map of Stockholm downtown.

computationally efficient method for calculating the maximum likelihood estimate of the wave parameters. The application of the SAGE algorithm for channel estimation is outlined in [20], [21]. In order to enhance its resolution ability, the Doppler frequency of the waves is also estimated [20]. The SAGE algorithm requires detailed knowledge of the response of the measurement system in order to return accurate estimates of the wave parameters. For this purpose, the complex radiation pattern of each array element has been measured in an anechoic chamber. The impulse response of the measurement equipment has also been measured by connecting the transmitter and the receiver with a cable. Both the measured radiation patterns and the impulse response have been included in the SAGE algorithm.

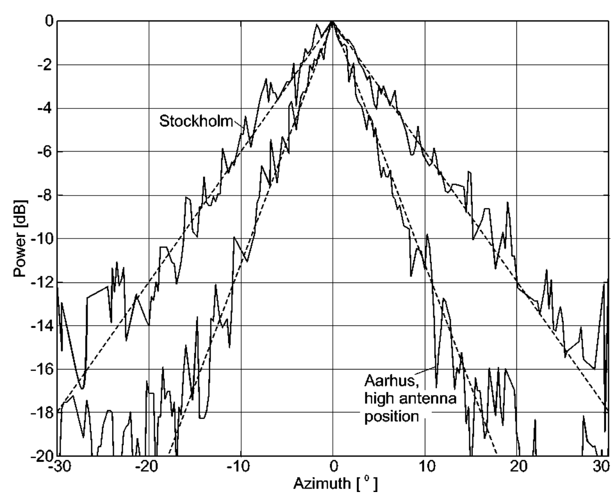

Fig. 4. Example of estimated PAS obtained in Aarhus and Stockholm.

IV. Power Spectra

A. Power Azimuth Spectrum

Two examples of the estimated PAS from measurements in Aarhus and Stockholm are illustrated in Fig. 4. The azimuth 0° corresponds to the azimuth towards the MS. In both cases the incident power is highly concentrated around 0° even though the measurements are obtained in a non-LOS situation. This indicates that a significant fraction of the received power propagates

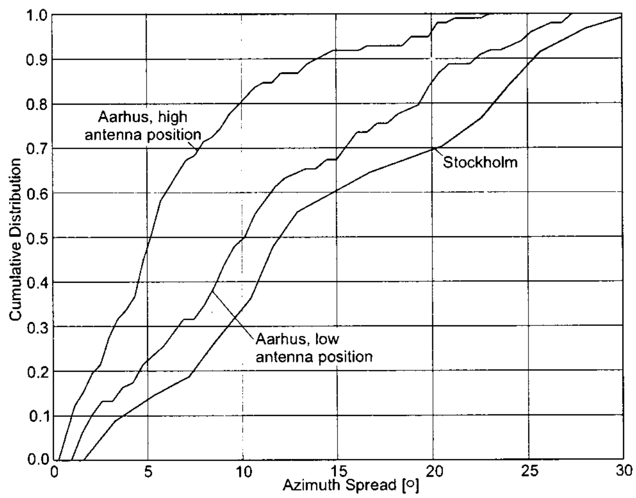

Fig. 5. Empirical cumulative distribution function of the estimated AS's.

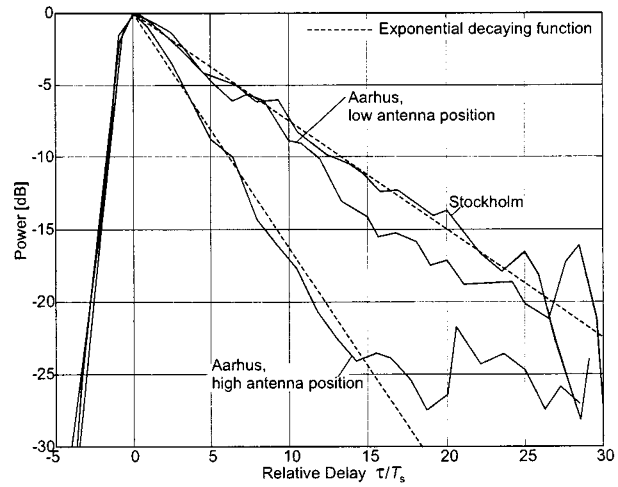

Fig. 6. Estimated PDS obtained in Aarhus and Stockholm. Sample time $T_s = 122$ ns.

from the MS to the BS via rooftop diffractions. It is furthermore observed that the Laplacian function

$$P_A(\phi) \propto \exp\left(-\sqrt{2}\frac{|\phi|}{\sigma}\right), \qquad \text{for } \phi \in [-180^\circ; +180^\circ] \tag{17}$$

matches the estimated PAS for signal levels higher than -12 dB. Notice that $\sigma \simeq \sigma_A$ under the assumption that $\sigma_A \ll 180^\circ$. For larger values of the AS, $\sigma_A < \sigma$ since the Laplacian function in (17) is truncated. Due to the limited dynamic range of the measurement system, it is not possible to determine whether the PAS continues to decrease for large azimuths in accordance with the tails of the Laplacian function. Additional PAS estimates from measurements made in Stockholm and Aarhus also support the thesis that the PAS is accurately modeled by a Laplacian function. Previous published results suggest to model the PAS with a truncated Gaussian function [24]. However, a comparison of the goodness of fit of the Laplacian and Gaussian function shows that the former gives the best match [22], [23].

The AS has been estimated for every 100λ segment along the different measurement routes in Aarhus and Stockholm (direction #2). The empirical cdf of the estimated AS is reported in Fig. 5 for different antenna heights. It can be observed that the AS changes significantly, but the shape of the PAS still follows a Laplacian function. In the proposed channel model, the PAS is therefore implicitly assumed to be conditioned on the AS for every 100λ segment. It can also be concluded from the measurements in Aarhus that the AS increases significantly when the antenna height is reduced. The 50% quantile of the AS equals 5° and 10° for the high and low antenna positions, respectively. Similarly, the 90% quantile of the AS equals 14° and 23°, respectively. The average received signal power drops at the same time by 8 dB. This loss is caused partly by an increased degree of obstruction between the MS and BS, which also explains the larger AS. The higher AS observed when the antenna height is low results in a larger decorrelation between the signals at the output of the antenna array compared to the high antenna position [10] and [25]. This result complies with Lee's model, which predicts that the correlation between two horizontally separated antennas decreases as the antenna height is reduced [25].

The AS is slightly higher in Stockholm compared to that obtained in Aarhus for the low antenna position although the antenna height was almost identical in both cases. The higher AS is conjectured to result because the environment in Stockholm is slightly more densely built up.

B. *Power Delay Spectrum*

The PDS has been investigated experimentally in numerous studies and is therefore only shortly discussed here. In accordance with [3], [4], and [6] among others, it is found that the PDS is accurately modeled by a one-sided exponential decaying function, i.e.,

$$P_D(\tau) \propto \begin{cases} \exp(-\tau/\sigma_D), & \text{for } \tau > 0 \\ 0, & \text{otherwise} \end{cases} \tag{18}$$

where σ_D is the DS as defined in Section II. Fig. 6 shows some examples of PDS estimated from the measurements made in Aarhus and Stockholm. The estimated PDS are shifted on the delay axis so their maxima corresponds to $\tau = 0$. It is observed that the one-sided exponential function closely matches the decaying behavior of the experimental curves for $\tau > 0$ and power levels above -20 dB. Outside this region other models may apply, e.g., the power law suggested in [29]. The first part of the PDS for $\tau < 0$, where it increases towards its maximum is not described by the exponential model and is simply neglected in the modeling. The well-known exponential model for the PDS is therefore adopted in the proposed channel model.

The DS has been estimated for every 100λ segment along the measurement routes in Stockholm and Aarhus. Fig. 7 shows the empirical cdf of the estimated DS's. It can be seen that the DS increases significantly as the antenna height is reduced in Aarhus. The 50% quantile of the DS equals 0.4 μs and 0.85 μs for the high and low antenna positions, respectively, while the 90% quantile DS equals 1.2 and 2.35 μs, respectively. Thus, the DS increases by approximately 50% when the antenna is lowered 12 m to the rooftop level. The same trend is reported in [28]. For comparison, the DS of the generally accepted COST207

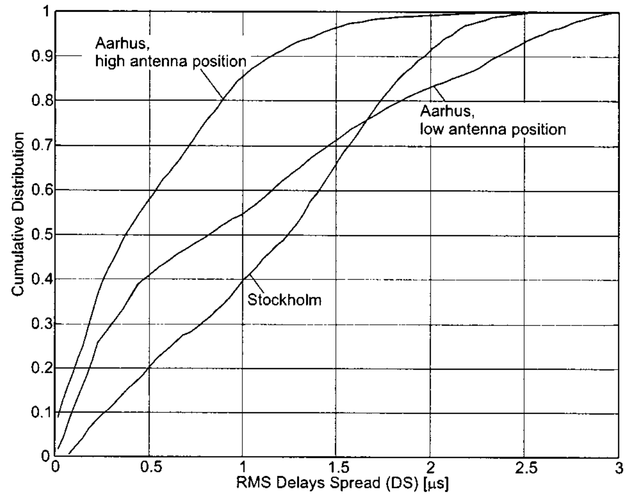

Fig. 7. Empirical cumulative distribution function of the estimated DS's.

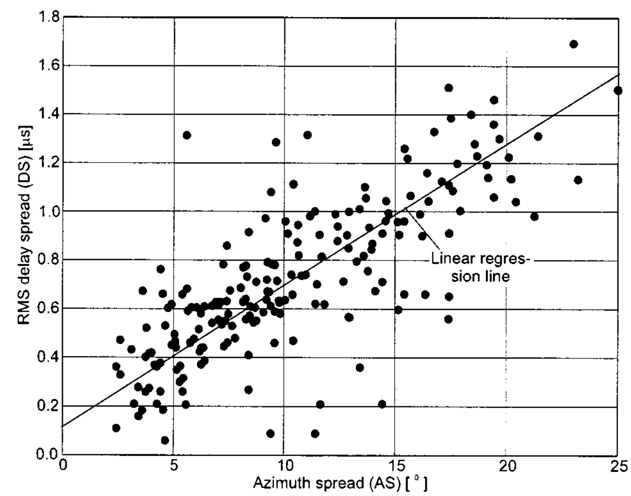

Fig. 8. Scatter plot of the estimated AS's and DS's obtained along the measurement routes in Stockholm (direction #2) and Aarhus.

typical urban model equals 1 μs [6]. The estimated DS's obtained in Stockholm and Aarhus with the low antenna position are of the same order.

C. Power Azimuth-Delay Spectrum

A comparison of the results in Sections IV-A and B shows that the estimated AS's and DS's are strongly related. In Aarhus, both DS and AS are found to increase significantly as the antenna height is reduced, and they are slightly higher in Stockholm compared to Aarhus. This indicates that the mechanisms leading to temporal and azimuthal dispersion are correlated. A scatter plot of the estimated DS's and AS's is shown in Fig. 8 for $N = 187$ different 100λ segments of the routes in both Stockholm and Aarhus. The correlation coefficient between the estimated DS's and AS's is computed as

$$\rho = \frac{\sum_{n=1}^{N}(\sigma_A[n] - \bar{\sigma}_A)(\sigma_D[n] - \bar{\sigma}_D)}{\sqrt{\sum_{n=1}^{N}(\sigma_A[n] - \bar{\sigma}_A)^2 \sum_{n'=1}^{N}(\sigma_D[n'] - \bar{\sigma}_D)^2}} \tag{19}$$

where $\sigma_D[n]$ and $\sigma_A[n]$ are the estimated DS and AS, respectively, for the nth segment, while $\bar{\sigma}_D$ and $\bar{\sigma}_A$ are the sample means of the estimated DS's and AS's, respectively. The correlation coefficient of the scatter plot in Fig. 8 is computed to be $\rho = 0.72$. The linear regression line is found to be $\sigma_D = (0.058\sigma_A + 0.12)$ [μs], where σ_A is expressed in degrees. The root-mean-square residual error is computed to be 0.18 μs, which indicates that the linear regression yields a reasonable approximation. These results furthermore indicate that the potential space and frequency diversity gains are highly correlated [25].

In order to gain further insight in the behavior of the power azimuth-delay spectrum $P(\phi, \tau)$, let us define the partial PAS at delay τ as

$$P_A(\phi; \tau) = \int_{\tau}^{\tau+\Delta\tau} P(\phi, \tau')\, d\tau' \tag{20}$$

where $\Delta\tau = 0.5$ μs. Similarly, the partial PDS at azimuth ϕ is defined as

$$P_D(\tau; \phi) = \int_{\phi}^{\phi+\Delta\phi} P(\phi', \tau)\, d\phi' \tag{21}$$

where $\Delta\phi = 5°$. The estimated partial PAS and PDS obtained for one 100λ segment in Aarhus are plotted in Fig. 9 for $\tau \in [0\text{ s}, 0.5\,\mu\text{s}, \cdots, 2.0\,\mu\text{s}]$ and $\phi \in [-12.5°, -7.5°, \cdots, 7.5°]$. All partial spectra are normalized so their maximum corresponds to 0.0 dB. A Laplacian function with 11° AS and an exponential function with 0.6 μs DS are also plotted for comparison. The partial PAS corresponding to large values of τ are close to the Laplacian function down to -10 dB, while those corresponding to short delays follow the Laplacian function down to -16 dB. All estimated partial PDS exhibit the same trend described by the exponentially decaying function for $\tau > 0$. Since the shape of the estimated $P_A(\phi; \tau)$ and $P_D(\tau; \phi)$ are invariant with τ and ϕ, respectively, we can assume that

$$P_A(\phi; \tau) \propto P_A(\phi) \quad \text{and} \quad P_D(\tau; \phi) \propto P_D(\tau). \tag{22}$$

In practice, the selected values of $\Delta\phi$ and $\Delta\tau$ are sufficiently small so from (22) the power azimuth-delay spectrum can be decomposed as

$$P(\phi, \tau) \propto P_A(\phi) P_D(\tau). \tag{23}$$

Notice that (23) does not imply that the mechanisms leading to azimuth dispersion and delay dispersion are uncorrelated. Recall that implicitly $P_A(\phi)$ is conditioned on the AS and $P_D(\tau)$ is conditioned on the DS. For a specific power azimuth-delay spectrum σ_A and σ_D are fixed, but the pair (σ_A, σ_D) changes from one 100λ segment to another. This means that in a simulation, σ_A and σ_D must be selected randomly while taking into account the correlation between them. The same conclusion can be drawn from investigations of many other 100λ segments in both Aarhus and Stockholm. Notice that, Spencer *et al.* apply a similar decomposition for an indoor propagation environment [26].

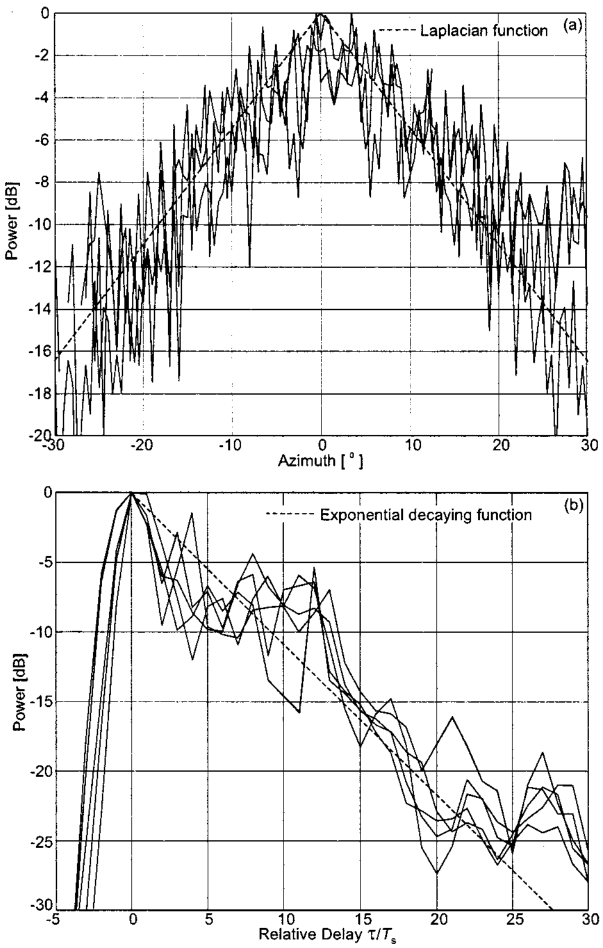

Fig. 9. Typical partial power spectra: (a) partial PAS at different delays and (b) partial PDS at different azimuths ($T_s = 122$ ns).

Notice that the proposed decomposition of the power azimuth-delay spectrum in (23) has been validated for typical urban environments only. For other classes of environments, such as bad urban, the decomposition might be invalid as argued in Section VII.

V. Probability Density Function of the Azimuths and Delays

A. Probability Density Function of the Azimuths

Fig. 10 shows a histogram of the estimated azimuths obtained in Aarhus for the high antenna position. The histogram is estimated from several 100λ segments with approximately the same AS, which in this case equals $\sigma_A = (5 \pm 0.5)^\circ$. Each bar represents an azimuth interval of 1°. The standard deviation computed from this histogram equals $\tilde{\sigma}_A = 6^\circ$. A Gaussian function with this standard deviation is also plotted in Fig. 10. The Gaussian function provides a good match, except for the tails of the histogram $(|\phi| > 12^\circ)$. In order to test the hypothesis of a Gaussian azimuth pdf the chi-square goodness of fit test is applied [27]. The T statistics of this test are computed by considering the interval $[-12^\circ; +12^\circ]$ corresponding to $[-2\tilde{\sigma}_A; +2\tilde{\sigma}_A]$. This interval represents 95% of the estimated azimuths assuming that they are Gaussian distributed. The T statistic is chi-square distributed with $k - m - 1$ degrees of freedom, where $k = 25$ is the number of considered azimuth intervals and $m = 2$ is the number of estimated parameters (mean and variance of the Gaussian function). The p value is computed to be $p = P\{\chi^2_{k-m-1} > T\} = 0.83$. Thus, for a confidence level larger than 0.83, the hypothesis that the azimuths are Gaussian distributed is rejected. From an engineering point of view, the p value is sufficiently high so that we can approximate $f_A(\phi)$ by a Gaussian pdf. The Gaussian pdf is also found to yield an accurate description of the azimuth histogram obtained in Stockholm and Aarhus with the low antenna position.

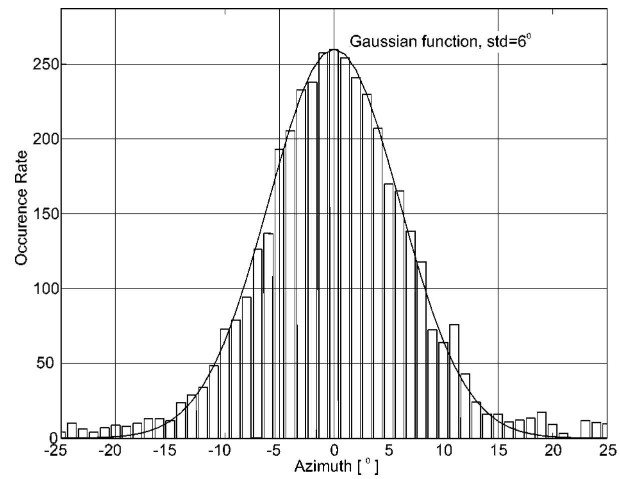

Fig. 10. Histogram of the estimated azimuths obtained in Aarhus with the antenna located 12 m above the rooftop level.

Comparing the results in Fig. 10 with Clarke's model, which assumes an uniform azimuth pdf at the MS, it is observed that there is a major difference between the azimuth pdf at the BS and the MS [14]. Consequently, the spatial correlation functions at the BS and MS also differ [10]. For two spatially separated antennas to be uncorrelated, half of a wavelength is normally required at the MS [14], [15], while 10–20 wavelengths are required at an elevated BS antenna depending on the AS [25].

The relation between the standard deviation of the azimuths $(\tilde{\sigma}_A)$ and the AS (σ_A) is investigated in the following. The pair $\{\tilde{\sigma}_A, \sigma_A\}$ is estimated for every 100λ segment along the different measurement routes in Aarhus and Stockholm. Based on these estimates, the proportionality factor between the two quantities is obtained by using a least squares estimation. The result of this analysis is shown in Table I. It can be observed that the proportionality factor is on the order of 1.23–1.42, so that in general $\tilde{\sigma}_A$ is slightly higher than σ_A.

B. Probability Density Function of the Delays

Different models describing the pdf $f_D(\tau)$ of the relative delays have been published in the literature. Turin proposed to model the delays as points generated by a nonhomogeneous Poisson process [3] or a modified Poisson process based on a two-state Markov model. The latter model better characterizes clustering of waves [4].

Fig. 11 shows a histogram of the estimated delays obtained in Aarhus with the high antenna position. A visual inspection reveals that the exponential function (solid curve) fits well to the histogram for delays larger than zero. A chi-square goodness of fit test has been applied to test the hypothesis that the delays

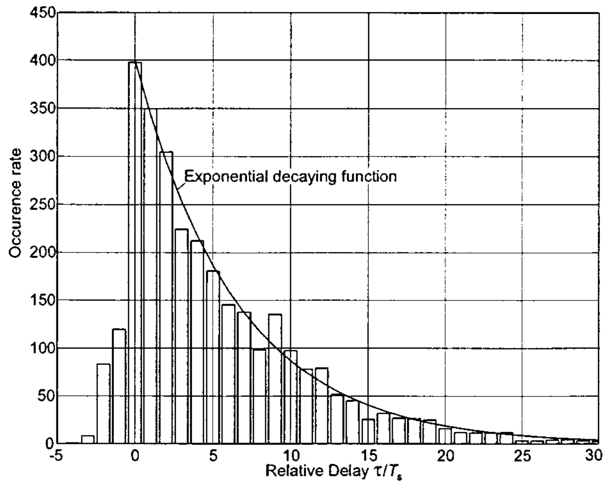

Fig. 11. Histogram of estimated delays obtained in Aarhus with the antenna positioned 12 m above the rooftop level.

lying within the interval $\tau/T_s \in [0, 1, \cdots, 25]$ are exponentially distributed. The p value is computed to be $p = P\{\chi^2_{k-m-1} > T\} = 0.78$, with $k - m - 1 = 26 - 1 - 1 = 24$ degrees of freedom. The p value is on the same order as that obtained for the chi-square test for the azimuth distribution. Consequently, it is reasonable to approximate $f_D(\tau)$ by an exponential pdf with standard deviation $\tilde{\sigma}_D$. The exponential pdf also provides a good approximation of the delay histograms obtained in Stockholm and Aarhus with the low antenna position.

The proportionality factor between the standard deviation $\tilde{\sigma}_D$ of the delays and the DS σ_D is investigated by estimating the pair $\{\tilde{\sigma}_D, \sigma_D\}$ for every 100λ segment along the different measurement routes. The result of this analysis is summarized in Table I. Here, the proportionality factor is on the order of 1.17–1.41, so in general the standard deviation of the delays is found to be slightly higher than the DS.

VI. Expected Power Versus Azimuth and Delay

A. Expected Power Conditioned on Azimuth

The estimated expected power conditioned on the azimuth is illustrated in Fig. 12. The estimate is obtained by averaging over several 100λ segments, where the AS is approximately the same, $\sigma_A = (5.0 \pm 0.5)^\circ$. As a consequence of the model assumptions, the expected power conditioned on azimuth can be expressed as

$$E\{|\alpha|^2 \,|\, \phi\} \propto P_A(\phi)/f_A(\phi) \tag{24}$$
$$\propto \exp\left(\frac{\phi^2}{2\tilde{\sigma}_A^2} - \sqrt{2}\frac{|\phi|}{\sigma_A}\right). \tag{25}$$

The second line results when the PAS is Laplacian and the azimuth pdf is Gaussian. Notice that the function in (25) exhibits a local maximum at 0° corresponding to the direction towards the MS and two local minima at $\phi^+_{\min} = \sqrt{2}\tilde{\sigma}_A^2/\sigma_A$ and $\phi^-_{\min} = -\sqrt{2}\tilde{\sigma}_A^2/\sigma_A$. For azimuths $|\phi| > \phi^+_{\min}$, (25) increases rapidly since the Gaussian function, $f_A(\phi)$, converges towards zero. The function (25) is also plotted in Fig. 12 for $\tilde{\sigma}_A = 1.38\sigma_A$ and $\sigma_A = 5^\circ$ according to the results in Table I. It is observed that the approximation error between (25) and the estimated curve is less than 1.2 dB for $|\phi| < \phi^+_{\min}$. For $|\phi| > \phi^+_{\min}$ the estimate of $E\{|\alpha|^2 \,|\, \phi\}$ is associated with a large uncertainty since only a few waves are present at these azimuths as seen from Fig. 10. For implementation of a radio channel simulator it is therefore suggested to truncate (25) so that $E\{|\alpha|^2|\phi\} = E\{|\alpha|^2 \,|\, \phi^+_{\min}\}$ for $|\phi| > \phi^+_{\min}$. This approximation also makes sense from a physical point of view since the power is not suddenly expected to start increasing with $|\phi|$.

TABLE I
Relation Between the Standard Deviation of Azimuths and AS and the Standard Deviation of Delays and DS

Environments	$\tilde{\sigma}_A$	$\tilde{\sigma}_D$
Aarhus, high antenna position	$1.38\sigma_A$	$1.17\sigma_D$
Aarhus, low antenna position	$1.42\sigma_A$	$1.41\sigma_D$
Stockholm, direction #2	$1.23\sigma_A$	$1.24\sigma_D$

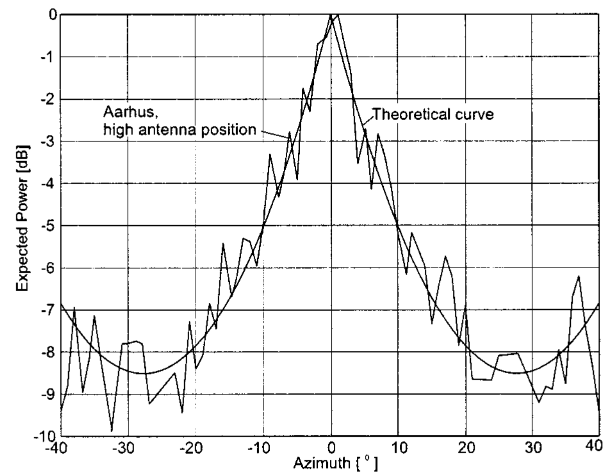

Fig. 12. Estimated conditional expected power versus azimuth. The theoretical function in (25) is plotted for $\tilde{\sigma}_A = 1.38\sigma_A$.

Estimates of $E\{|\alpha|^2 \,|\, \phi\}$ have been obtained for many other 100λ segments in both Stockholm and Aarhus, and an agreement similar to the one presented in Fig. 12 has been observed.

B. Expected Power Conditioned on Delay

The estimated expected power conditioned on delay obtained from measurements in Aarhus is shown in Fig. 13. According to the proposed channel model in Section II, the following relationship applies: $E\{|\alpha|^2 \,|\, \tau\} \propto P_D(\tau)/f_D(\tau)$. Assuming that both $P_D(\tau)$ and $f_D(\tau)$ are exponential decaying functions, we obtain

$$E\{|\alpha|^2 \,|\, \tau\} \propto \exp\left(-\tau\frac{\tilde{\sigma}_D - \sigma_D}{\tilde{\sigma}_D\sigma_D}\right). \tag{26}$$

The function (26) is plotted in Fig. 13 for $\tilde{\sigma}_D = 1.17\sigma_D$ and $\sigma_D = 1.0\ \mu$s according to the results in Table I. A visual inspection reveals that (26) fits the experimental curve within ± 1.6 dB in the range $\tau/T_s \in [0, 1, \cdots, 25]$. For larger delays, the deviation between the experimental data and the theoretical curve

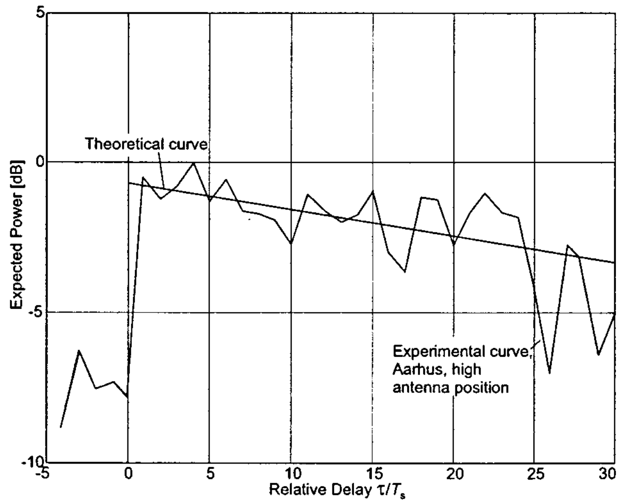

Fig. 13. Estimated conditional expected power versus delay. The exponential function in (26) is plotted for $\tilde{\sigma}_D = 1.17\sigma_D$.

tends to increase. The larger deviation may be caused by estimation errors since only a few waves are observed at large delays and consequently the estimate of the expectation becomes less accurate. Expressed in decibels, (26) is a straight line with a slope equal to

$$\frac{\partial E\{|\alpha|^2 \,|\, \tau\}_{\mathrm{dB}}}{\partial \tau} = -4.3\frac{\tilde{\sigma}_D - \sigma_D}{\tilde{\sigma}_D \sigma_D} \quad [\mathrm{dB/s}]. \tag{27}$$

With the selected parameter values the slope equals -0.62 dB/μs. In comparison, the slope of the linear regression fitted to the experimental data in the range $\tau/T_s \in [0, 1, \cdots, 25]$ is -0.54 dB/μs. Thus, both values are close together.

VII. Power Azimuth-Delay Spectrum in Bad Urban Environments

The results presented in Sections IV–VI are characteristic for the dispersive behavior of the radio channel in a uniformly built-up urban area, referred to as typical urban. In nonuniform urban environments consisting of a mixture of open areas and densely built up zones with a large variety of different building heights, the dispersion in the radio channel may likely look completely different. This type of environment is referred to as bad urban. In the following, measurement results obtained in Stockholm with the antenna array pointing in direction #1 are presented. Fig. 14 pictures a typical example of the PDS and PAS observed when the MS is located south of the river (see the map of Stockholm in Fig. 3).

The PDS and PAS are composed of two clusters. Cluster #1 corresponds to the power coming directly from the MS. Cluster #2 is contributed by waves which propagate over the river and are then reflected on building fronts located on the north side of the river back to the BS. Cluster #2 is delayed by 4.27 μs relative to cluster #1, which corresponds to a distance of 1281 m. This is a typical behavior observed for different locations of the MS on the south side of the river. However, when the MS is located on the north side of the river, typically, only one cluster of waves is received.

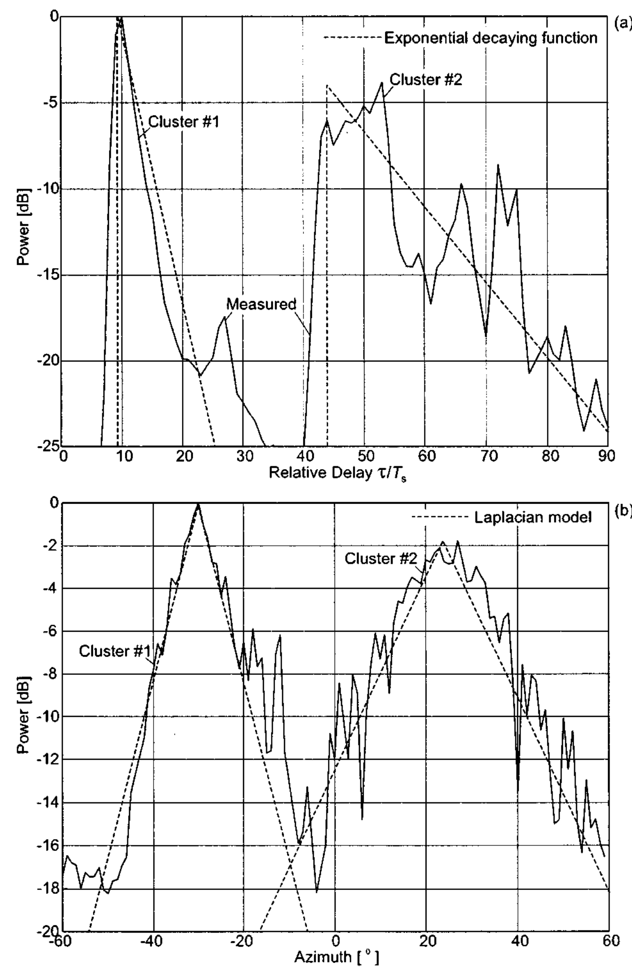

Fig. 14. Example of a PDS and PAS obtained in Stockholm for antenna direction #1 (bad urban). Sample time $T_s = 122$ ns.

For comparison, two one-sided exponential functions with DS equal to 0.4 and 1.3 μs for cluster #1 and #2, respectively, have been plotted in Fig. 14(a). Two Laplacian functions with AS 7.6° and 12.1° are also shown in Fig. 14(b). The separation in delay and azimuth between the two clusters changes as the MS moves from one location to another. For this type of environment the power delay-azimuth spectrum cannot be decomposed as the product of the PAS and the PDS, as it can be assumed for the typical urban area. The reason for this is that the power impinging from azimuths around $-30°$ is related only to the first cluster in the PDS.

The PAS in Fig. 14 is interesting from an array processing point of view since it poses a number of opportunities and problems. First, it is clear that the two clusters can be effectively separated by conventional beamforming techniques resulting in a significant reduction of the DS. On the other hand, the large AS makes it very difficult to apply conventional null-steering techniques to cancel out an interferer. However, the large AS results in highly decorrelated signals at the output of the antenna array, which makes it possible to mitigate fast fading by means of space diversity techniques.

A. Simple Multicluster Model

As already mentioned, it is observed from Fig. 14 that the PAS and PDS can be approximated by a superposition of two Laplacian functions and two exponential decaying functions, respectively. However, situations with more than two clusters may also appear, although such a behavior has not been observed in the investigated environments. It is therefore suggested to model the power azimuth-delay spectrum in a more general form as

$$P(\phi,\tau)=\sum_{k=1}^{K}P_k(\phi,\tau). \quad (28)$$

Here, $P_k(\phi,\tau)$ represents the contribution from cluster #k to $P(\phi,\tau)$ and K is the number of clusters. A similar two-cluster $(K=2)$ model for the PDS is part of the COST207 bad urban model [6]. Thus, (28) can be seen as a simple extension of this model to include azimuthal dispersion.

VIII. Conclusion

A stochastic model is proposed which includes both azimuthal and temporal dispersion in the radio propagation channel. For typical urban environments, it is found that the PAS and PDS are accurately modeled by a Laplacian function and a one-sided exponential decaying function, respectively. A positive correlation is observed between the AS and DS. Hence, propagation environments leading to high AS also yield high DS and vice versa. It is found that both the AS and DS increase by approximately 50% as the BS antenna is lowered by 12 m down to rooftop level. Depending on the antenna height, the median AS is in the range 5°–15° and the median DS lies in the range 0.4–1.3 μs. From a receiver point of view, the dependency between AS and DS means that the potential gains which can be achieved by using frequency and space diversity are highly correlated too. Investigations of the partial PAS and PDS show that the power azimuth-delay spectrum can be expressed less a proportionality constant as the product of the PDS and PAS. The pdf's of the azimuth and delay of the impinging waves are found to closely match a Gaussian function and a one-sided exponential decaying function, respectively. This means that the expected power of the waves conditioned on delay equals an exponential function and the expected power conditioned on azimuth equals a Laplacian function divided by a Gaussian function.

In bad urban environments, the power impinging at the BS is frequently found to come from two distinct main directions and not only from the direction towards the MS as observed in typical urban environments. A more appropriate description of dispersion in the radio channel in bad urban environments is therefore obtained by using a two-cluster model, where the PAS is described by a sum of two Laplacian functions and the PDS is the sum of two exponential decaying functions. The power azimuth-delay spectrum cannot be expressed as a product of the PDS and PAS in this case. Situations with more than two clusters may also be realistic.

It is believed that the proposed stochastic channel model provides a simple method for generating realistic input signals to array processing algorithms in urban environments. This basically means that more robust algorithms can be designed and tested under realistic conditions before they are finally implemented in an operating BS.

Acknowledgment

The authors wish to thank S. Larsen, F. Frederiksen, K. Olesen, and P. Leth-Espensen for building the testbed and assisting during the measurement campaign. J. Bach Andersen's comments on the manuscript are greatly appreciated. Also, the authors thank J.-E. Berg and H. Asplund from Ericsson Radio Systems AB for their help during the measurement campaign in Stockholm. Finally, the authors appreciate the useful comments from the anonymous reviewers.

References

[1] A. F. Naguib, A. J. Paulraj, and T. Kailath, "Capacity improvement with base-station antenna arrays in cellular CDMA," *IEEE Trans. Veh. Technol.*, vol. 43, pp. 691–698, Aug. 1994.

[2] *Algorithms and Antenna Array Recommendations*, May 1997. Public deliverable from the European ACTS, TSUNAMI II project. Deliverable code: AC020/AUC/A1.2/DR/P/005/b1.

[3] G. Turin, F. Clapp, T. Johnston, S. Fine, and D. Lavry, "A statistical model of urban multipath propagation," *IEEE Trans. Veh. Technol.*, vol. 21, pp. 1–9, Feb. 1972.

[4] H. Suzuki, "A statistical model for urban radio propagation," *IEEE Trans. Commun.*, vol. 25, pp. 673–680, July 1977.

[5] H. Hashemi, "Simulation of the urban radio propagation channel," *IEEE Trans. Veh. Technol.*, vol. 28, pp. 213–225, Aug. 1979.

[6] *Information Technologies and Sciences—Digital Land Mobile Radio Communications*, Sept. 1988. Commission of the European Communities, COST207.

[7] R. B. Ertel, P. Cardieri, K. W. Sowerby, T. S. Rappaport, and J. H. Reed, "Overview of spatial channel models for antenna array communication systems," *IEEE Personal Commun.*, pp. 10–21, Feb. 1998.

[8] P. Eggers, "Angular dispersive mobile radio environments sensed by highly directive base station antennas," in *IEEE Proc. Personal, Indoor and Mobile Radio Communications (PIMRC'95)*, Sept. 1995, pp. 522–526.

[9] P. A. Bello, "Characterization of randomly time-variant linear channels," *IEEE Trans. Commun. Syst.*, vol. CS-11, pp. 360–393, Dec. 1963.

[10] K. I. Pedersen, P. E. Mogensen, and B. H. Fleury, "Spatial channel characteristics in outdoor environments and their impact on BS antenna system performance," in *IEEE Proc. Veh. Technol. Conf. (VTC'98)*, Ottawa, Canada, May 1998, pp. 719–724.

[11] J. Liberti and T. Rappaport, "A geometrically based model for line-of-sight multipath radio channels," in *IEEE Proc. Veh. Technol. Conf. (VTC96)*, May 1996, pp. 844–848.

[12] M. Lu, T. Lo, and J. Litva, "A physical spatio-temporal model of multipath propagation channels," in *IEEE Proc. Veh. Technol. Conf. (VTC97)*, May 1997, pp. 810–814.

[13] O. Nørklit and J. B. Andersen, "Diffuse channel model and experimental results for antenna arrays in mobile environments," *IEEE Trans. Antennas Propagat.*, vol. 46, pp. 834–840, June 1998.

[14] R. H. Clark, "A statistical theory of mobile radio reception," *Bell Labs Syst. Tech. J.*, vol. 47, pp. 957–1000, July–Aug. 1968.

[15] W. C. Jakes, *Microwave Mobile Communications*. New York: IEEE Press, 1974.

[16] T. Aulin, "A modified model for the fading signal at a mobile radio channel," *IEEE Trans. Veh. Technol.*, vol. 28, pp. 182–203, Aug. 1979.

[17] J. G. Proakis, *Digital Communications*, 3rd ed. New York: McGraw-Hill, 1995.

[18] *Wideband Direct-Sequence CDMA (WCDMA), Part I: System Description*, Nov. 1997. Concept Group Alpha ETSI SMG2 UMTS.

[19] J. A. Fessler and A. Hero, "Space-alternating generalized expectation-maximization algorithm," *IEEE Trans. Signal Processing*, vol. 42, pp. 2664–2677, Oct. 1994.

[20] K. I. Pedersen, B. H. Fleury, and P. E. Mogensen, "High resolution of electromagnetic waves in time-varying radio channels," in *IEEE Proc. Personal, Indoor and Mobile Radio Communications (PIMRC'97)*, Sept. 1997, pp. 650–654.

[21] B. H. Fleury, M. Tschudin, R. Heddergott, D. Dahlhaus, and K. I. Pedersen, "Channel parameter estimation in mobile radio environments using the SAGE algorithm," *IEEE J. Select. Areas Commun.*, vol. 17, pp. 434–450, Mar. 1999.

[22] K. I. Pedersen, P. E. Mogensen, and B. H. Fleury, "Power azimuth spectrum in outdoor environments," *IEE Electron. Lett.*, vol. 33, pp. 1583–1584, Aug. 1997.

[23] U. Martin, "A directional radio channel model for densely built-up urban areas," in *Proc. 2nd EPMCC*, Bonn, Germany, Oct. 1997, pp. 237–244.

[24] F. Adachi, M. Feeny, A. Williamson, and J. Parsons, "Crosscorrelation between the envelopes of 900 MHz signals received at a mobile radio base station site," *Proc. Inst. Elect. Eng.*, vol. 133, pt. F., pp. 506–512, Oct. 1986.

[25] W. C. Y. Lee, *Mobile Communications Engineering*. New York: McGraw-Hill, 1982.

[26] Q. Spencer, M. Rice, B. Jeffs, and M. Jensen, "A statistical model for angle of arrival in indoor multipath propagation," in *IEEE Proc. Veh. Technol. Conf. (VTC97)*, May 1997, pp. 1415–1419.

[27] S. M. Ross, *Introduction to Probability and Statistics for Engineers and Scientists*. New York: Wiley, 1987.

[28] P. Mogensen, P. Eggers, and J. Elling, "Propagation measurements in city area for GSM small cells," in *Proc. 4th Nordic Seminar on Digital Mobile Radio Communications*, Oslo, Norway, June 1990.

[29] J. B. Andersen and P. Eggers, "A heuristic model of power delay profiles in landmobile communications," in *Proc. URSI Int. Symp. Electromagnetic Theory*, Sydney, Australia, Aug. 1992, pp. 55–57.

Klaus Ingemann Pedersen received the M.Sc. degree in electrical engineering in 1996 from Aalborg University, Aalborg, Denmark. He is currently working towards the Ph.D. degree at Aalborg University.

During 1996, he was with Lucent Technologies Bell Labs Innovations, where he was involved in the design of CDMA receivers. His current research interests are channel modeling for antenna arrays and vector receivers for DS-CDMA systems.

Preben E. Mogensen received the M.Sc. and Ph.D. degrees in electrical engineering in 1988 and 1996, respectively, from Aalborg University, Aalborg, Denmark.

Since 1988, he has been with Aalborg University, where he is now an Associate Research Professor at the Center for Personkommunication (CPK). He is leading the Cellular Systems research group at CPK. Since 1995, he has also been a part-time System Consultant for Nokia Telecommunications. His current research areas are adaptive antenna technology and radio resource management for second- and third-generation cellular systems.

Bernard H. Fleury was born in Porrentruy, Switzerland, on March 28, 1954. He received the diploma in electrical engineering and mathematics in 1978 and 1990, respectively, and the Ph.D. degree in electrical engineering in 1990 from the Swiss Federal Institute of Technology Zurich (ETHZ), Switzerland.

From 1978 to 1985, he was a Teaching and Research Assistant at the Communication Technology Laboratory (CTL) and a Teaching and Research Assistant from 1988 to 1992 at the Statistics Seminar, ETHZ. In 1992, he joined the CTL again where he headed the Spread Spectrum Team beginning in 1994. In 1996, he spent seven months as a Research Professor at the Center for PersonKommunikation (CPK), Aalborg University, Aalborg, Denmark. Since 1997, he has been a Guest Professor in Digital Communication at CPK. His current fields of interest include stochastic modeling of the mobile radio channel, high-resolution methods for the estimation of the radio channel, advanced techniques for joint channel parameter estimation, and data detection/decoding in spread-spectrum multiuser communication systems.